Molecular-dynamics study of ductile and brittle fracture in model noncrystalline solids

M. L. Falk*
Department of Physics, University of California, Santa Barbara, California 93106
(Received 20 July 1998; revised manuscript received 9 February 1999)

Molecular-dynamics simulations of fracture in systems akin to metallic glasses are observed to undergo embrittlement due to a small change in interatomic potential. This change in fracture toughness, however, is not accompanied by a corresponding change in flow stress. Theories of brittle fracture proposed by Freund and Hutchinson indicate that strain rate sensitivity is the controlling physical parameter in these cases. A recent theory of viscoplasticity in this class of solids by Falk and Langer further suggests that the change in strain rate sensitivity corresponds to a change in the susceptibility of local shear transformation zones to applied shear stresses. A simple model of these zones is developed in order to quantify the dependence of this sensitivity on the interparticle potential. [S0163-1829(99)09733-7]

I. INTRODUCTION

This paper presents simulations in which a small change in interparticle potential leads to a qualitative change in ductility. Section II describes the simulation technique and observations. Section III details a technique for calculating a quantitative measure of local nonaffine deformation which is applicable to materials with no crystalline order, and using this technique pinpoints those areas of the material which are undergoing some molecular level rearrangement akin to a dislocation. Section IV relates this observed change in ductility to the particular change in interparticle potential. This final section discusses the simulations in terms of current phenomenological theories of brittle and ductile behavior due to Freund and Hutchinson[1] and a theory of this mechanism of molecular level rearrangement in noncrystalline materials developed by Falk and Langer which we shall refer to as FL.[2] Finally, a simplified microscopic model is analyzed. This model directly relates the interparticle potential to the parameter which controls deformation in FL and the change of fracture toughness observed in the simulations. The model also explains the observations of Srolovitz, *et al.* relating these regions to ''τ defects'' in previous metallic glass simulations.[3,4]

The concepts of brittleness and ductility are central to any understanding of failure in solids. The most developed first-principles theories of ductility are rooted in the dynamics of dislocations in crystalline solids.[5–7] Although it has been conjectured that an analog to a crystal dislocation exists in noncrystalline solids,[8] it remains unclear how to make the direct connection to molecular level phenomena necessary for these theories to be useful in quantitatively understanding transitions between brittle and ductile behavior in disordered materials. In fact, it is not at all clear that a dislocation model of this sort is the most appropriate way to understand materials without regular structure although these materials are observed to undergo similar brittle-ductile transitions to their crystalline counterparts. It is conjectured here that dislocation concepts are not the most natural way to describe noncrystalline solids and theories of ''shear transformation zones'' (STZ's) as first considered in the literature on metallic glasses[9–14] are developed as a natural way to understand some of the basic physics of brittle versus ductile fracture.

II. SIMULATIONS OF BRITTLE AND DUCTILE FRACTURE IN A NONCRYSTALLINE SOLID

This section describes a series of molecular-dynamics (MD) simulations of fracture in a simple, two-dimensional amorphous solid. While these simulations are clear examples of change in ductility induced by a change in interparticle potential the important point here is not simply to differentiate between brittle and ductile behavior, but rather to establish a connection between this particular change in the potential and a change the observed fracture toughness.

From a practical standpoint these studies of brittle and ductile behavior are relevant in the context of several different disordered and amorphous materials. The simulated system is most similar to metallic glasses which have been observed to undergo transitions between ductile and brittle behavior both as a function of temperature and due to small amounts of dilute crystallization produced during annealing.[15–18] Similar transitions are also critical to the processing of colloidal ceramic systems. These claylike materials undergo brittle-ductile transitions due to changes in salt content, i.e., changes in interparticle interactions.[19] Issues of brittleness and ductility are also crucial for the production of high-strength polycrystalline metallic alloys in which such transitions have been studied experimentally with respect to temperature and loading rate.[20]

In modeling interparticle interactions a Lennard-Jones (LJ) potential is employed. This is consistent with previous investigations which have been carried out in the context of metallic glasses.[3,4,21–23] While more sophisticated models of interactions within metals exist many, such as the Johnson potential for iron[24] or the model potential for copper and zirconium employted by Deng, Argon, and Yip,[23] have a basic form similar to that of the LJ potential. The use of a simplified potential can be justified here since these simulations seek to elucidate how a well controlled change in potential affects fracture behavior rather than exploring the accuracy of a particular potential.

Despite the simplicity of the LJ potential, the similarity of the results of these simulations to experiments carried out in metallic glasses is striking. First, as in the simulations, both brittle and ductile fracture are observed in metallic glasses at low temperature depending on composition. Typically these

glasses display a pseudo-cleavage fracture mode which involves significant flow at the crack tip evidenced by vein patterns.[15] However, compositional changes can lead to brittle modes of fracture in which such flow is not in evidence.[25] Some Pd-Si glasses have even been observed to display the ''mirror,'' ''mist,'' ''hackle'' behavior typical of the extremely brittle oxide glasses.[26] Though a transitional temperature to this brittle mode is seen in many metallic glasses, some have been observed to experience pseudocleavage at all observed temperatures even as low as 76 K.[25]

Secondly, as in the simulations, metallic glasses at low temperature are observed to experience changes in fracture toughness independent of flow stress. Tests of the dynamic fracture response and the onset of flow in Pd-Si and Fe-P-C glasses show a distinct crossover from a thermally activated to an athermal mechanism for fracture and flow at temperatures of 273 and 473 K, respectively.[27,28] In the high-temperature regime flow and fracture are observed to follow the same trend when strain rate is varied. But, in the low-temperature regime analogous to these simulations, the flow stress is observed to be independent of strain rate while the fracture stress is strain rate dependent.[15] In these simulations a change in potential produces a change in fracture toughness that is not accompanied by a corresponding change in the flow stress. This can be related theoretically to a change in strain rate sensitivity independent of the flow stress, and will be discussed in detail in Sec. IV.

A. Methodology

The simulated systems consisted of 90 000 particles in two dimensions interacting via a two-body potential. In order to avoid problems of local crystallization, a polydisperse collection of particles was simulated. The system was composed of eight different species in equal proportion with radii $r_1, r_2, \ldots, r_8$ such that

$$r_\alpha = 1.1 r_{\alpha-1}, \quad \sum_{\alpha=1}^{8} \pi r_\alpha^2 = 8\pi (d_0/2)^2. \tag{2.1}$$

Thus, the total volume of the collection was the same as if the particles were all of radius $d_0/2$, and the system is roughly comparable to a single component system in which the rest spacing between two molecules is d_0. All quantities will be given in terms of dimensions for which d_0 is the length scale. Therefore in these units $d_0 = 1$. The masses of all particles were taken to be $m = 1$ in these units.

The intermolecular potential was different in the two simulations. In the simulation which displayed more ductile behavior the potential was a standard Lennard-Jones 6-12 potential

$$U_{\alpha\beta}^{\mathrm{LJ}}(r) = e\left[\left(\frac{r_\alpha + r_\beta}{r}\right)^{12} - 2\left(\frac{r_\alpha + r_\beta}{r}\right)^{6}\right], \tag{2.2}$$

where r is the interparticle distance and r_α and r_β are the radii of the two particles. e, the depth of the energetic minimum of the two particle interaction, is unity in our units. Note, this is not the standard form of writing the LJ potential, which is typically written in terms of the hardcore radius $a_\alpha = 2^{-1/6} r_\alpha$. This expression is, however, equivalent and will facilitate the introduction of the second potential to which it will be compared.

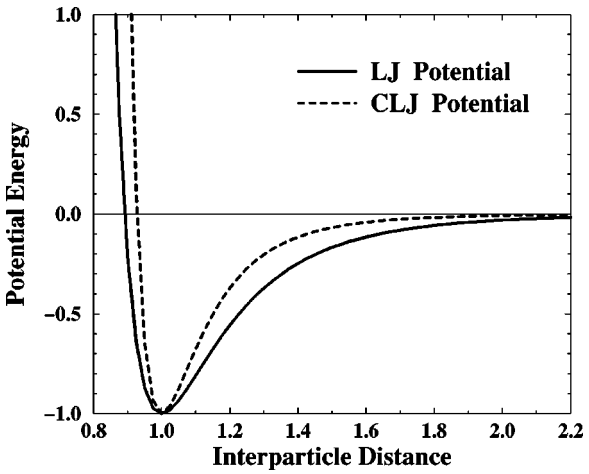

FIG. 1. The LJ and CLJ potentials. Energy is given in units of e. Interparticle distance is given in units of d_0.

The simulation which displayed more brittle behavior employed a potential which will be refered to as the compressed Lennard-Jones (CLJ) potential because it is the Lennard-Jones potential rescaled around the center of the potential well

$$U_{\alpha\beta}^{\mathrm{CLJ}}(r) = U_{\alpha\beta}^{\mathrm{LJ}}[\lambda r + (1-\lambda)(r_\alpha + r_\beta)]. \tag{2.3}$$

Note that the standard LJ potential is recovered when $\lambda = 1$. Furthermore, $\lambda \to 0$ corresponds to a mean field limit in which every particle interacts with every other particle equivalently, and $\lambda \gg 1$ is the limit of solely nearest neighbor interactions. For the second simulation the parameter λ was chosen to be 1.5. This means that width of the potential well was smaller by 33%, and, consequently, the effective range of interaction was also shortened compared to the standard LJ interaction. For the sake of comparison Fig. 1 shows both potentials. In both cases interactions were cut off at a range of $d_c \approx 2.2 d_0$.

All times are given in units of $t_0 = d_0\sqrt{m/e}$. This unit of time is approximately equivalent to one molecular vibrational period.

The initial amorphous systems were created by taking 10 000-molecule systems and equilibrating them using a sequential MD algorithm with periodic boundary conditions, a Nose-Hoover thermostat[29–31] and Parrinello-Rahman barostat.[32,33] The equations of motion and time constants for the thermostat and barostat were the same as those in FL.[2] The time step in the simulations was taken to be $0.01 t_0$. The systems were held at low temperature $kT = 0.01e$ for 5000 time steps at zero pressure, then the pressure was raised to $10e/d_0^2$ over the course of 1000 time steps and lowered again over an equal period of time. Subsequently the samples were allowed to equilibrate at zero pressure for 1000 time steps. This procedure created close-packed samples. The LJ sample was observed to have a Young's modulus of 34 and a shear modulus of 10; the CLJ sample was observed to have a

Young's Modulus of 39 and a shear modulus of 12. These 10 000-molecule samples were then used to create larger systems by replicating the small system in a 3×3 array.

The larger systems were simulated via a parallel MD algorithm based on a spatial decomposition method.[34] In order to create the initial conditions for the fracture simulations, the large system was equilibrated for 100 time steps while held at a very low temperature, $kT=0.001e$. A crack was then introduced into the sample. This was accomplished by imposing displacements as determined by the analytical solution for a straight crack in an elastic medium loaded below the ideal critical stress. The faces of the crack were marked so that the top face would not interact with the bottom face to prevent the crack from healing. The outer boundaries of the system were held fixed while the simulation was again run for 20 000 time steps holding the temperature constant to allow the system to relax.

In the fracture simulations no thermostat or barostat was employed. To drive the crack, an initial velocity gradient was imposed across the sample, and the top and bottom surfaces were constrained to move apart vertically such that the side closer to the crack would separate at a strain rate of $0.0001t_0^{-1}$ and the side farthest from the crack would not move apart at all. The horizontal motion of these surfaces was unconstrained. The left and right surfaces were constrained not to move in the horizontal direction, though their vertical motion was unconstrained.

A strain rate of $0.0001t_0^{-1}$ corresponds to a physical strain rate on the order of 10^8 s^{-1}. While this may seem high compared to typical laboratory values, the time for a sound wave to traverse the sample is $\approx 300t_0$. The time for stresses in the sample to equilibrate will be several times this duration. The fact that the time for a soundwave to traverse the sample multiplied by the strainrate is $\approx 0.03 \ll 1$ implies that the system was loaded nearly quasistatically. That is to say that the loading rate was slower than the elastic response time, although the loading may not be slow when compared to the time scale for plastic response. Of course, if the crack begins to propagate strain rates near the tip may be significantly higher.

B. Observations

Figure 2 shows the average stress measured during both simulations. In order to better compare the two systems, the stresses are given in units of the critical stress for initial failure of a perfectly brittle solid with the identical elastic properties

$$\sigma_c = \sqrt{\frac{GE}{\pi a}}. \tag{2.4}$$

Here we assume that the system can be treated as a crack in an infinite medium. E is Young's modulus, a is the initial length of the crack, and G is the energy release rate, which can be expressed as a surface energy and a dissipation per unit crack extension,

$$G = 2\gamma + G_{\text{diss}}. \tag{2.5}$$

For an ideally brittle solid all the elastic energy released goes into the creation of new surface, $G_{\text{diss}}=0$. γ was measured by taking a sample of the material in MD, slicing it along an arbitrary plane and measuring the change in potential energy. The value of γ is $1.04e/d_0$ in the CLJ system and $0.94e/d_0$ in the LJ system, thus $\sigma_c^{\text{ideal}}=0.68e/d_0^2$ in the ductile system, and $0.70e/d_0^2$ in the brittle system.

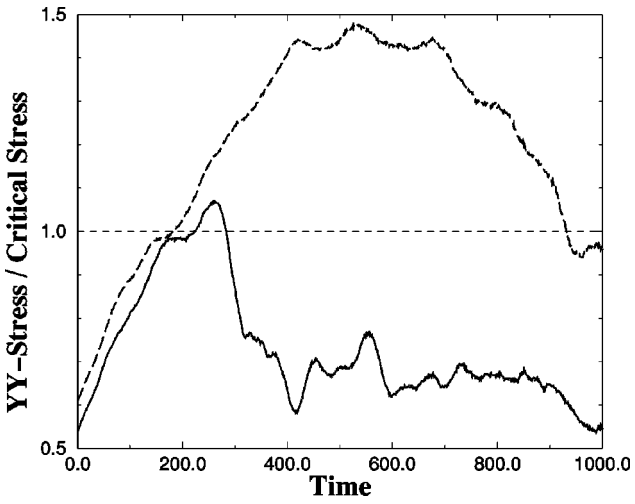

FIG. 2. Stress averaged throughout the sample versus time for the CLJ (solid) and LJ (dashed) simulations. The higher stress for the onset of fracture in the LJ case implies increased dissipation. Stresses are given in units of the critical stress for failure of an ideally brittle material with the same elastic properties. Time is given in units of $d_0\sqrt{m/e}$.

Two notable differences are observed between the simulations. (i) In the CLJ simulation, some modest amount of energy was dissipated and the crack began to propagate at about 7% above the ideal brittle critical stress, but in the LJ simulation fracture did not proceed until the stress was 48% above this value. This means that for the CLJ case the ratio of energy dissipated to the energy expended creating surface is 0.14, while for the LJ case this ratio is 1.19. (ii) In the CLJ simulation, once the crack began to propagate, the stress in the system sharply dipped as the crack moved through the system at speeds reaching 30% of the shear wave speed. Throughout this process the crack tip remained atomically sharp. The process stopped short of releasing all the stress because the crack arrested. In the LJ case, however, the crack tip blunted significantly. In this simulation, the stress remained high while voids nucleated ahead of the tip. The speed of the ductile crack, while difficult to measure due to the mechanism of propagation, stayed well below the speed of the CLJ crack.

III. QUANTIFYING LOCAL DEFORMATION

The simulation which utilized the CLJ potential resulted in markedly more brittle behavior than the simulation that utilized the LJ potential. In order to address why this particular change in potential resulted in differing amounts of deformation near the crack tip the underlying mechanism of deformation must be established. Work by Argon and Spaepen suggests that localized deformations, or ''shear transformation zones,'' are responsible for rearrangements in these amorphous materials. This section undertakes an examination of the microscopic nature of the plastic rearrange-

ment in order to determine if this is indeed the case for this set of simulations. These microscopic observations also serve to differentiate the simulations performed here from similar investigations of fracture undertaken in crystals[36,37] where plasticity is observed to result from dislocations emitted from the crack tip or activated in the vicinity of the crack.

A. Definition of $D^2_{\min}$

In a perfect crystal, dislocations can be readily identified by their characteristic stress fields or as regions of anomalously high potential energy. In glasses, however, such analyses are difficult due to inhomogeneities frozen into the structure. Furthermore, it is not clear that any analog of crystalline dislocations exists in noncrystalline solids. For these reasons, a different scheme must be developed to identify regions which deform in a nonaffine way and thereby observe what sort of microscopic structures play the role of dislocations in these materials.

To identify local rearrangements from a set of molecular positions and subsequent displacements the closest possible approximation to a local strain tensor is computed in the neighborhood of any particular molecule. The neighborhood is defined in this case by the interaction range d_c. The local strain is then determined by minimizing the mean square difference between the the actual displacements of the neighboring molecules relative to the central one, and the relative displacements that they would have if they were in a region of uniform strain ε_{ij}. That is, we define

$$D^2(t,\Delta t)=\sum_n \sum_i \left\{ r_n^i(t)-r_0^i(t)-\sum_j (\delta_{ij}+\varepsilon_{ij}) \times [r_n^j(t-\Delta t)-r_0^j(t-\Delta t)] \right\}^2, \tag{3.1}$$

where the indices i and j denote spatial coordinates, and the index n runs over the molecules within the interaction range of the reference molecule, $n=0$ being the reference molecule. $r_n^i(t)$ is the ith component of the position of the nth molecule at time t. Here D^2 is calculated for displacements at time t taking the configuration at time $t-\Delta t$ as the reference configuration. We then find the ε_{ij} which minimizes D^2 by calculating:

$$X_{ij}=\sum_n [r_n^i(t)-r_0^i(t)]\times[r_n^j(t-\Delta t)-r_0^j(t-\Delta t)], \tag{3.2}$$

$$Y_{ij}=\sum_n [r_n^i(t-\Delta t)-r_0^i(t-\Delta t)] \times[r_n^j(t-\Delta t)-r_0^j(t-\Delta t)], \tag{3.3}$$

$$\varepsilon_{ij}=\sum_k X_{ik}Y_{jk}^{-1}-\delta_{ij}. \tag{3.4}$$

The minimum value of $D^2(t,\Delta t)$ is then the local deviation from affine deformation during the time interval $[t-\Delta t,t]$. Here we are interested in the deviation relative to the configuration at $t=0$, and, therefore, we compute the minimum of $D^2(t,t)$. This quantity shall be refered to as $D^2_{\min}$.

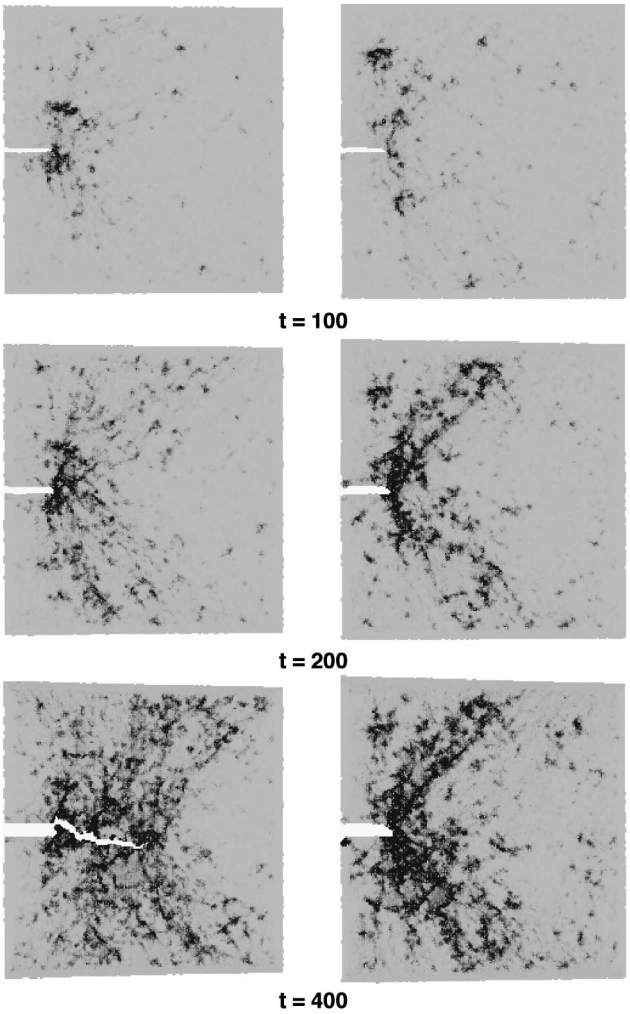

FIG. 3. Frames from the CLJ (left) and LJ (right) fracture simulations. In each set the frames are shaded by the parameter $D^2_{\min}$ defined in Eq. (3.1). Dark regions have undergone the highest amount of nonaffine rearrangement. The shading saturates when $D^2_{\min}=1$. Movies of these simulations are available via the internet.[35]

B. Molecular level observations

$D^2_{\min}$ serves as a diagnostic for identifying where local rearrangements have taken place. Figures 3 and 4 are shaded by the value of $D^2_{\min}$ over the interval from $t=0$ to the current time. It is immediately apparent that much more nonaffine rearrangement takes place in the LJ simulation than in the CLJ simulation. In addition, there seem to develop preferred directions along which deformation takes place. These slip bands which nucleate at the crack tip in the LJ simulation are clear signs that the dynamics of the plastic response and the resulting propagating shear modes are crucial aspects of the problem.

Figure 5 shows one example of a local region before and after rearrangement. This rearrangement took place in the early stages of the ductile simulation prior to significant blunting a small distance in the y direction from the tip. The arrows denote the sense of the externally applied shear in this region calculated by knowing the asymptotic stress field near a crack tip. The figure illustrates that these regions appear to be of the type discussed by Spaepen as ''flow defects''[12] or in other contexts as ''shear transformation zones.'' That is,

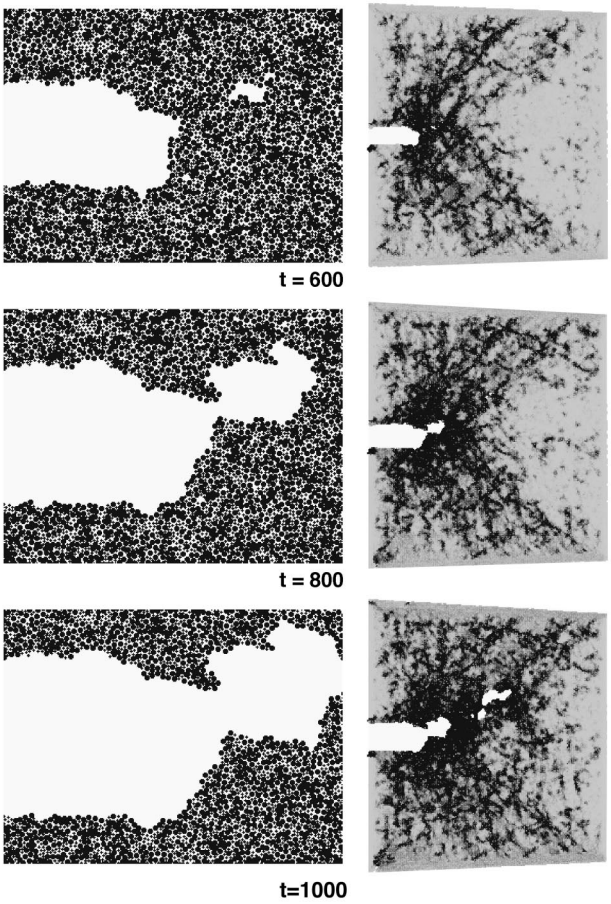

FIG. 4. Frames from the LJ simulation showing the nucleation and growth of a void in the vicinity of the crack tip. The frames on the left are close-ups of the crack tip. The frames on the right are shaded as in Fig. 3. This simulation is available in movie format via the internet.[35]

the region seems to consist of roughly 10–20 particles, the rearrangements seem to be local, and the ''defect'' is not mobile in the same sense as a dislocation. Srolovitz, Maeda, Vitek, and Egami established that these rearranging regions correspond structurally to ''τ defects,'' regions of anomalously high local shear stress.[3,4] The following section will further explore why these regions are ''τ defects'' and how both the high local stresses and deformation dynamics arise from the particulars of the intermolecular potentials.

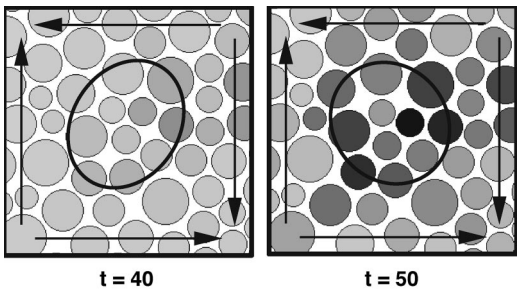

FIG. 5. A local region before and after nonaffine rearrangement. The molecules are shaded by $D^2_{\min}$, the amount of nonaffine rearrangement. The arrows denote the approximate direction of the externally applied shear. The ovals are included solely as guides for the eye.

IV. ANALYSIS

These simulations beg the question as to why this change in interatomic potential leads to the observed change in ductility. Unfortunately, the current lack of a detailed understanding of the microscopics of plasticity in noncrystalline materials will rule out a detailed first-principles theory of such transitions at this stage. However, some important connections can be made between these simulations and current theories of dynamic fracture and the theory of viscoplasticity in amorphous solids presented in FL.[2] In addition, toward the end of this section a simplified model of the molecular rearrangements at the heart of the viscoplasticity theory will be detailed. This model serves to illustrate how a first-principles theory may eventually be developed.

A. Macroscopic: brittle-ductile behavior

We begin by considering the theory of high strain-rate crack growth proposed by Freund and Hutchinson.[1] In this theory the plastic strain rate is considered negligible below some shear stress σ_{flow} and above this stress the strain rate $\dot{\varepsilon}_s^{\text{pl}}$ rises linearly:

$$\dot{\varepsilon}_s^{\text{pl}} = \dot{\varepsilon}_t + \dot{\varepsilon}_0(\sigma_s - \sigma_{\text{flow}})/\mu. \tag{4.1}$$

Here μ is the shear modulus, σ_s is the applied shear stress, $\dot{\varepsilon}_t$ is the flow rate at yield, and $\dot{\varepsilon}_0$ characterizes the strain rate sensitivity. Furthermore $\dot{\varepsilon}_t \ll \dot{\varepsilon}_0$ and the effect of $\dot{\varepsilon}_t$ will not be important for the purpose of this analysis. Using an assumption of strain rate dominance, the theory finds that the energy release rate of the crack is velocity dependent. Furthermore, the energy release rate of the brittle crack diverges at both high and low velocity. Between these two diverging limits there exists a velocity at which the energy release rate of the crack is a minimum. According to this model the crack cannot propagate when driven at less than this minimum energy release rate. The value of the minimum energy release rate depends on the specifics of the plastic response described in Eq. (4.1). By Freund and Hutchinson's analysis

$$\frac{G_{\min}}{G^c_{\text{tip}}} \approx 1 + \mathcal{C}\frac{\dot{\varepsilon}_0}{\sigma^2_{\text{flow}}}, \tag{4.2}$$

where G^c_{tip} is the bare fracture toughness near the tip and $\mathcal{C}$ is a proportionality constant which depends on the shear modulus, density, and G^c_{tip}. [NB: We will ignore a second term proportional to $\dot{\varepsilon}_t/\dot{\varepsilon}_0$ for reasons discussed above.]

In the context of this theory we can ask what would cause one material to propagate a brittle crack while another admits a more ductile mode of failure. Since a given mode of failure can only result if a propagating solution exists, we can conjecture that the ductile failure mode results when the propagating brittle solution becomes, for some reason, inaccessible. For brittle behavior to have resulted from the narrowing of the interparticle potential then, the minimum energy release rate should have decreased when the potential well width was narrowed. This further implies that the narrowing of the potential either caused a decrease in $\dot{\varepsilon}_0$, the

sensitivity of the strain rate to a change in applied stress, or an increase in σ_{flow}, the critical stress for appreciable plastic flow.

The simplest explaination for the increase in brittleness would be that the narrowing of the potential raised the critical stress for plastic flow. This is not the case. Bulk measurements of σ_{flow} obtained by simulating the two systems in periodic boundary conditions with zero applied pressure and a constant applied shear strain rate reveal no significant differences. $\sigma_{\text{flow}} \approx 0.4(e/d_0^2)$ for both systems. This implies that a change in the flow stress is not the cause of the embrittlement in the simulations presented here.

Returning for a moment to the Freund and Hutchinson model, we note that having eliminated σ_{flow} as the responsible parameter for the change in the mode of failure, we must consider the parameter $\dot{\varepsilon}_0$. This parameter corresponds to the sensitivity of the strain rate to an applied stress above the flow stress (essentially an inverse viscosity)

$$\dot{\varepsilon}_0 = \mu \left. \frac{\partial \dot{\varepsilon}_s^{\text{pl}}}{\partial \sigma_s} \right|_{\sigma_{\text{flow}}^+}. \tag{4.3}$$

In order to explore why such a change in $\dot{\varepsilon}_0$ might arise we will now consider a somewhat simplified version of the theory of viscoplasticity in amorphous solids developed in FL.

B. Mesoscopic: viscoplasticity in amorphous solids

In the model of viscoplasticity discussed in FL the plastic flow is both rate and history dependent. The history dependence of the model enters through a set of state variables which describe the density of ''shear transformation zones'' (STZ) of the type described in Sec. III B. These STZ's are theorized to be essentially two-state systems and are assumed to have a definite orientation. That is to say that STZ's that are particularly susceptible to deformation under one sense of shear may not be susceptible to another, and when an STZ undergoes a transition it changes orientation so as to be susceptible to an opposite applied shear stress. For the sake of simplification the STZ's are assumed to be either perfectly aligned with the applied stress or antialigned with the applied stress. Furthermore, the first few nonlinear terms which describe the dynamics of these STZ's are conjectured. These terms represent an assumption that inelastic work done on the system may generate new regions or eliminate existing regions.

In FL the rate of plastic strain is related to the rate at which STZ's transform between their two states,

$$\dot{\varepsilon}_s^{\text{pl}} = V_z \Delta\varepsilon [R_+ n_+ - R_- n_-], \tag{4.4}$$

where V_z is the typical volume of a region, $\Delta\varepsilon$ is the increment of local strain due to an individual transformation, $n_\pm$ are the population densities of STZ's in each of the two states, and $R_\pm$ are functions of the stress describing the rate at which transitions occur between the two states. The evolution equations of $n_\pm$ are written in terms of a master equation[38,39]

$$\dot{n}_\pm = R_\mp n_\mp - R_\pm n_\pm - C_1(\sigma_s \dot{\varepsilon}_s^{\text{pl}}) n_\pm + C_2(\sigma_s \dot{\varepsilon}_s^{\text{pl}}), \tag{4.5}$$

where C_1 and C_2 are constants associated with the nonlinear terms which determine the rate of STZ annihilation and creation. The equations of motion have two steady states: a ''jammed'' or ''hardened'' state below the critical stress for plastic flow and a flowing state above this stress. For the flowing steady state

$$n_\pm = \frac{C_2}{C_1} \mp \frac{1}{V_z \Delta\varepsilon C_1 \sigma_s}. \tag{4.6}$$

The specifics of the choice of the functions $R_\pm$ and their dependence on the stress are important for determining the time dependence of the plastic flow. In FL the transition rates are written as volume activated processes. That is, the rates are written in the form

$$R_\pm = R_0 \exp\left[- \frac{\Delta V^*(\pm \sigma_s)}{v_f} \right], \tag{4.7}$$

where for the purpose of this analysis we will assume R_0 to be a constant attempt frequency, v_f is a free volume per particle, and ΔV^* is a free volume needed to activate a transition. The volume needed to activate the transition ΔV^* is a function of the applied shear stress which is chosen to have the simplest one parameter functional form for which the volume is assured to be non-negative.

$$\Delta V^*(\sigma_s) = V_0^* \exp(-\sigma_s/\bar{\mu}), \tag{4.8}$$

where V_0^* is the free volume needed to activate a transition at zero stress, and $\bar{\mu}$ is a modulus which characterizes the sensitivity of the activation volume to the applied stress. Note that in general $V_0^* \gg v_f$ and these rates are negligible unless $\sigma_s \approx +\bar{\mu}$. Since we are considering the material response around $\sigma_s = +\sigma_{\text{flow}}$, we are in a regime where $R_+ \gg R_-$.

Taking this formulation of the transition rates into account, we can consider the rate of deformation described by Eq. (4.4) in the the steady-state flow regime of Eq. (4.6):

$$\dot{\varepsilon}_s^{\text{pl}} \approx V_z \Delta\varepsilon R_+ n_+ = \frac{R_+}{C_1} [\sigma_{\text{flow}}^{-1} - \sigma_s^{-1}], \tag{4.9}$$

where $\sigma_{\text{flow}} = (C_2 V_z \Delta\varepsilon)^{-1}$. So, we can evaluate $\dot{\varepsilon}_0$ in Eq. (4.3) using Eqs. (4.7)–(4.9) to be

$$\dot{\varepsilon}_0 = \frac{\mu}{C_1 \sigma_{\text{flow}}^2} R_0 \exp\left[- \frac{V_0^*}{v_f} e^{-\sigma_{\text{flow}}/\bar{\mu}} \right]. \tag{4.10}$$

This last equation provides a first clue as to which aspect of the microscopic behavior is responsible for the observed change from ductile to brittle failure. First, note that we can reasonably neglect the prefactors to the exponential since the effect of changes in these terms will be substantially less dramatic. Furthermore, the ratio V_0^*/v_f, which was already noted to be a large number, is expected to depend primarily on the relative sizes of the particles which are the same in both systems. Since the possibility of a substantial change in σ_{flow} has been ruled out, the only remaining parameter in this expression is $\bar{\mu}$. The double exponential causes $\dot{\varepsilon}_0$ to be

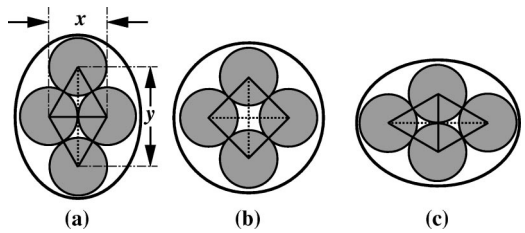

FIG. 6. Diagram of four identical interacting particles making a transition from one stable configuration to another. The middle configuration is the saddle-point configuration for this transition.

suppressed by a factor of $\exp(-V_0^*/v_f)$ when $\bar{\mu}$ becomes large. Moreover Eq. (4.10) is most sensitive to changes in $\bar{\mu}$ when $\bar{\mu} \approx \sigma_{\text{flow}}$. The investigations of analogous amorphous systems via computer simulation in FL suggested that $\bar{\mu}$ does indeed fall in this range.

The observation that $\dot{\varepsilon}_0$ is highly sensitive to changes in $\bar{\mu}$ means that the sensitivity of the material flow rate to a change in applied shear stress is highly dependent on the sensitivity of the deformable regions (STZ's) in the solid. Relating this to Freund and Hutchinson's fracture model this implies that the observed change from ductile to brittle failure seems to be due to a corresponding change from ''floppier'' to ''stiffer'' weak regions in the solid. But while the viscoplasticity theory leads us to these conclusions it does not elucidate how one might quantify these ideas and relate them to the molecular potentials.

C. Microscopic: simplified model of a two-state region

This idea of ''floppy'' or ''stiff'' STZ's can be made more meaningful by considering a simplified model of molecular rearrangements. The model should be consistent with the observations of Argon, Spaepen, and co-workers, i.e., it should be capable of rearranging in a local way,[9–13] and also with the observations made by Srolovitz and co-workers, i.e., it should be a ''τ defect.''[3,4] Figure 6 shows the most stripped-down model of how these two-state systems must look on the molecular level, four molecules interacting via a two-body interatomic potential. Since this unit is embedded in the solid it is constrained from undergoing translation or rotation. For particular choices of the interatomic potential this four-molecule unit is inherently a two-state system. That is to say that for a Lennard-Jones or similar potential the energy is minimized by having as many bonds near the equilibrium bond length as possible. In this system there are two degenerate ground states, illustrated in Figs. 6(a) and 6(c), in which five of the six bonds are of this length.

Because transitions between the two states of our four-body unit are associated with the development of strain in the solid, the material response must depend upon the rates at which these transitions occur. At high temperatures the transition rates are dominated by rare thermal events which occur only as $\exp(-\Delta U/kT)$, where ΔU is the energy difference between the ground state and the saddle point illustrated in Fig. 6(b). This is exactly the approach used to describe the time dependent strain in theories of deformation kinetics such as those of Eyring, Spaepen, and Argon.[9,13,38,39] Such a formalism is not of use here. In the present system ΔU is on order unity while kT is three orders of magnitude smaller. Physically this means transitions will be driven rather than thermally activated. This is, of course, cause for alarm. The statistical approach of the theories of deformation kinetics in high-temperature systems utilized the statistical nature of the energetic fluctuations to discern a time scale. How can a statistical theory be developed when these fluctuations are not relevant? Instead, consider the solid to be composed of an ensemble of these two-state systems, some small fraction of which are close to a free volume induced transition. By using this ensemble picture it is possible to preserve the rare-event aspects of transition state theory in order to extract a relevant time scale.

The concept of a free volume induced transition has been mentioned here, but although this concept has been discussed in some detail in FL, the molecular details of such a transition have not been discussed. In particular, it is necessary to be able to calculate $\Delta V^*(\sigma_s)$, the shear stress dependent free volume needed to activate the transition. The following paragraphs will attempt to answer the following question: For the model two-state system, constrained by its surroundings to a certain area, what is the maximum shear that it can support before being driven into a different state? If this question can be answered, then, given some applied shear stress, it will be possible to determine the free area (our two-dimensional equivalent of free volume) at which a region will become unstable.

With this picture in mind let us consider in some detail what is going on physically. We can parametrize the energy of the four-particle system by only two parameters, its x and y dimensions, if we constrain it from rotating, translating or deforming in an asymmetric way:

$$\mathcal{U}(x,y) = U(x) + U(y) + 4U\left(\frac{1}{2}\sqrt{x^2+y^2}\right). \tag{4.11}$$

Here U can be any two-particle potential, but we will concern ourselves with U_{LJ} and U_{CLJ} described in Sec. II A. Furthermore, consider the case when the area (two-dimensional volume) of the system remains constant by imposing the constraint $A = xy$. We can define a local equivalent shear stress

$$\Sigma_s(x,y) = \frac{1}{2}\left(\frac{1}{y}\frac{\partial \mathcal{U}}{\partial x} - \frac{1}{x}\partial\frac{\mathcal{U}}{\partial} y\right). \tag{4.12}$$

At this point it is possible to understand why such two-state STZ's would be visible as ''τ defects,'' the regions of anamolously high shear stress described by Srolovitz *et al.*[3,4] Consider the condition for the lowest energy of the configuration

$$\frac{d\mathcal{U}}{ds} = \frac{A}{\sqrt{x^2+y^2}}\left(\frac{1}{y}\frac{\partial \mathcal{U}}{\partial x} + \frac{1}{x}\frac{\partial \mathcal{U}}{\partial y}\right) = 0, \tag{4.13}$$

where the path of constraint is traversed by a unit speed curve parameterized by s such that $ds^2 = dx^2 + dy^2$. We immediately note that the condition for equilibrium is **not** the same as the condition for zero shear stress. In general these two conditions are not simultaneously satisfiable. It is important to note that an exception to this, i.e., a case in which the lowest energy configuration has no shear stress, is the case

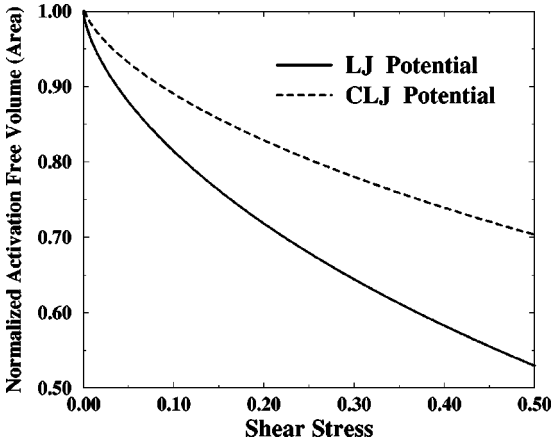

FIG. 7. The activation free volume (area) at shear stress Σ_s divided by the activation free volume (area) at zero applied shear stress $A_f(\Sigma_s)/A_f(0)$. The activation free volume (area) corresponds to the excess volume at which the four particle system illustrated in Fig. 6 becomes unstable to the applied shear. Stresses are given in units of e/d_0^2.

where the molecules interact only via nearest neighbor interactions. This is particularly interesting in light of the simulations since the limit where $\lambda \gg 1$ in Eq. (2.3) is the limit of solely nearest neighbor interactions. Therefore, we expect that the CLJ potential ($\lambda = 1.5$), which resulted in increased brittleness in the simulations, should show lower levels of internal shear stresses and fewer ''τ defects'' than the LJ potential ($\lambda = 1$) which resulted in increased ductility. Thus, the microscopic model strongly suggests that the range of the intermolecular potential is crucial in determining whether these STZ's are visible as ''τ defects.''

We return now to the question of when the two-state STZ will become unstable to an externally applied shear stress. The condition for instability can be written

$$\frac{d\Sigma_s}{ds} = \frac{1}{\sqrt{x^2+y^2}}\left(x\frac{\partial \Sigma_s}{\partial x} - y\frac{\partial \Sigma_s}{\partial y}\right) = 0, \qquad (4.14)$$

where we have again traversed the path of constraint by a unit speed curve. We can now define the equivalent of a free volume in our system $A_f = A - A_0$. Here A_0 is the equilibrium area of the four-body system at zero applied shear stress $\approx \sqrt{3}(d_0^2)$. Figure 7 shows the value of $A_f(\Sigma_s)/A_f(0)$ at which instability sets in for values of the shear stress Σ_s. In order to illustrate the suppression of ΔV^*, and by analogy A_f, as the stress is raised to the flow stress, Fig. 7 spans a range of shear stresses up to our observed flow stresses in the fracture samples. This graph looks suggestively similar to the form guessed in Eq. (4.8). In actual fact, however, in the vicinity of $\Sigma_s = 0$, A_f is a power law and not an exponential decay. This suppression of the activation volume can be related to values for $\bar{\mu}$ in FL. The activation area at $\Sigma_s = 0.4$ is 58% of its value at zero in the LJ case and 74% in the CLJ case; this corresponds to $\bar{\mu}_{\mathrm{LJ}} = 0.73$ and $\bar{\mu}_{\mathrm{CLJ}} = 1.3$. Thus, longer range intermolecular potentials correspond to a solid with ''floppier'' two-state regions. This result is significant since longer range potentials also implied larger local stresses, and the existence of ''τ defects.'' As expected from the previous analysis, the toy model with the CLJ potential has a higher value of $\bar{\mu}$ and, therefore, corresponds to a solid with ''stiffer'' two-state regions. This is in keeping with our expectations since ''stiffer'' two-state regions should also correspond to a lower value of $\dot{\varepsilon}_0$ and, therefore, by Freund and Hutchinson's model to a lower minimum energy release rate for brittle fracture from Eq. (4.2). The CLJ solid is observed to undergo brittle fracture.

The analysis presented here is clearly only a first step toward a rigorous first-principles theory of brittle-ductile transitions in noncrystalline solids. Future investigations will hopefully allow more explicit connections to be made between the molecular level structures which are quantifiable via diagnostics such as D^2_{min} and the observed fracture behavior. Progress will require further developments in our understanding of the molecular physics of deformation in noncrystalline solids.

ACKNOWLEDGMENTS

I would like to acknowledge J.S. Langer for his guidance and encouragement, Alexander Lobkovsky for sharing his ideas and results regarding decohesion models, and A. S. Argon, B. L. Holian, M. Marder, and R. L. B. Selinger for helpful discussions. This work was supported by the U.S. DOE Grant No. DE-FG03-84ER45108 and the DOE Computational Sciences Graduate Fellowship Program. The work was also supported in part by National Science Foundation Grant No. CDA96-01954, Silicon Graphics Inc., and the Cornell Theory Center.

*Present address: Division of Engineering and Applied Sciences, Harvard University, Cambridge, MA 02138. Electronic address: falk@esag.harvard.edu

[1] L.B. Freund and J.W. Hutchinson, J. Mech. Phys. Solids **33**, 169 (1985).
[2] M.L. Falk and J.S. Langer, Phys. Rev. E **57**, 7192 (1998).
[3] D. Srolovitz, K. Maeda, V. Vitek, and T. Egami, Philos. Mag. A **44**, 847 (1981).
[4] D. Srolovitz, V. Vitek, and T. Egami, Acta Metall. **31**, 335 (1983).
[5] J.R. Rice and R. Thomson, Philos. Mag. **29**, 73 (1974).
[6] J.R. Rice, J. Mech. Phys. Solids **40**, 239 (1992).
[7] S.J. Zhou, A.E. Carlsson, and R. Thomson, Phys. Rev. Lett. **72**, 852 (1994).
[8] J.J. Gilman, J. Appl. Phys. **44**, 675 (1973).
[9] F. Spaepen, Acta Metall. **25**, 407 (1977).
[10] A.S. Argon, Acta Metall. **27**, 47 (1979).
[11] A.S. Argon and H.Y. Kuo, Mater. Sci. Eng. **39**, 101 (1979).
[12] F. Spaepen and A.I. Taub, *Les Houches Lectures XXXV on Physics of Defects* (North-Holland, Amsterdam, 1981), p. 133.
[13] A.S. Argon and L.T. Shi, Acta Metall. **31**, 499 (1983).
[14] V.A. Khonik and A.T. Kosilov, J. Non-Cryst. Solids **170**, 270 (1994).
[15] C.A. Pampillo, J. Mater. Sci. **10**, 1194 (1975).

[16] T.-W. Wu and F. Spaepen, Philos. Mag. B **61**, 739 (1990).
[17] W.L. Johnson, Appl. Phys. Lett. **225**, 35 (1996).
[18] C.J. Gilbert, R.O. Ritchie, and W.L. Johnson, Appl. Phys. Lett. **71**, 476 (1997).
[19] G.V. Franks and F.F. Lange, J. Am. Ceram. Soc. **79**, 3161 (1996).
[20] R.D. Noebe, C.L. Cullers, and R.R. Bowman, J. Mater. Res. **7**, 605 (1992).
[21] K. Maeda and S. Takeuchi, Phys. Status Solidi A **49**, 685 (1978).
[22] S. Takeuchi and K. Maeda, Key Eng. Mater. **13**, 749 (1987).
[23] D. Deng, A.S. Argon, and S. Yip, Philos. Trans. R. Soc. London, Ser. A **329**, 549 (1989).
[24] R.A. Johnson, Phys. Rev. **134**, A1329 (1964).
[25] C.A. Pampillo and D.E. Polk, Acta Metall. **22**, 741 (1974).
[26] T. Matsumoto and R. Maddin, Acta Metall. **19**, 725 (1971).
[27] H.S. Chen, H.J. Leamy, and M. Barmatz, J. Non-Cryst. Solids **5**, 444 (1971).
[28] R. Maddin and T. Matsumoto, Mater. Sci. Eng. **9**, 153 (1972).
[29] S. Nose, J. Chem. Phys. **81**, 511 (1984).
[30] S. Nose, Mol. Phys. **52**, 255 (1984).
[31] S. Nose, Mol. Phys. **57**, 187 (1986).
[32] M. Parrinello and A. Rahman, J. Appl. Phys. **52**, 7182 (1981).
[33] M. Parrinello and A. Rahman, J. Chem. Phys. **76**, 2662 (1982).
[34] S. Plimpton, J. Comput. Phys. **117**, 1 (1995).
[35] See AIP Document No. E-PAPS: PRBMDO-60-097933 for movie files. E-PAPS document files may be retrieved free of charge from our FTP server (http://www.aip.org/pubservs/epaps.html) or from ftp.aip.org in the directory /epaps/. For further information, e-mail: paps@aip.org or fax: 516-576-2223.
[36] S.J. Zhou, P.S. Lomdahl, R. Thomson, and B.L. Holian, Phys. Rev. Lett. **76**, 2318 (1996).
[37] F.F. Abraham, D. Brodbeck, R.A. Rafey, and W.E. Rudge, Phys. Rev. Lett. **73**, 272 (1994).
[38] H. Eyring, J. Chem. Phys. **4**, 283 (1936).
[39] A.S. Krausz and H. Eyring, *Deformation Kinetics* (Wiley, New York, 1975).